

Graphene plasmons and retardation: strong light-matter coupling

G. GÓMEZ-SANTOS and T. STAUBER

Departamento de Física de la Materia Condensada and Instituto Nicolás Cabrera, Universidad Autónoma de Madrid, E-28049 Madrid, Spain

PACS 73.21.Ac – Multilayers

PACS 42.25.Bs – Wave propagation, transmission and absorption

PACS 78.67.Wj – Optical properties of graphene

Abstract – We study the retardation regime of doped graphene plasmons, given by the nominal crossing of the unretarded plasmon and light-cone. In addition to modifications in the plasmon dispersion relation, retardation implies strong coupling between propagating light and matter, even for homogeneous graphene, which opens up the possibility of efficient plasmonics in simple graphene devices. We exemplify this enhancement in a double-layer configuration that exhibits *perfect* (if lossless) light transmissions across a classically forbidden region, providing a simpler analog of the corresponding phenomenon in perforated metal sheets. We also show that (broad) Fabry-Pérot resonances present without graphene turn into sharply peaked, quasi-discrete modes in the presence of graphene where graphene’s response function is given by the typical Fano lineshape.

Introduction. – In addition to its amazing transport and mechanical properties [1], graphene’s optical behavior is also notable. Absorption, for instance, has the experimentally observed [2, 3], universal value $\approx \pi\alpha$ for light in the visible spectrum, depending on the fine structure constant α , but not on material’s properties. Several proposals and/or realizations highlight graphene potential in optical and communication technologies, including resistive touchscreens of transparent and flexible displays, [4, 5], opto-electronic devices such as photodetector [6], broadband absorber [7], mode-locked laser due to current saturation [8], or as a highly efficient fluorescence quencher [9–15].

Doped graphene has attracted much attention recently as a suitable candidate for noble metal’s replacement in the active field of plasmonics [16–19]. In addition to their intrinsic importance as a probe for dynamics, graphene plasmons [20–22] (GPs) offer a number of advantages such as frequency tunability, long life-times, and spatial confinement due shorter (than light) wavelengths. They have been observed via electron energy loss spectroscopy [23, 24] and near-field nanoscopy. [25–27]

Unfortunately, GPs do not couple easily to propagating electromagnetic modes over most of its range due to the large momentum mismatch, complicating their manipulation. This problem could be overcome by breaking the conservation of parallel momentum either with con-

finer geometries [19, 28] or artificial periodicities [29–31]. However, there is a regime where even homogeneous GPs must couple strongly to (propagating) light: the retardation limit. It applies for frequencies below a characteristic crossover scale, which can be taken as the crossing between the nominal, unretarded GP dispersion and the light-cone. There, phenomena associated with strong light-graphene coupling take place.

Here, we demonstrate this enhanced light-graphene coupling and apply it to a double-layer graphene [32, 33] arrangement possessing *extraordinary transmission*. This term was originally coined to describe the enormous transmission experimentally observed through periodically perforated metal sheets [34–36], a situation where the naive expectation would have prescribed just the opposite. An explanation was provided in terms of the excitation of surface plasmons, with the result of enhanced transmission (*perfect* in the absence of absorption) through a nominally opaque region. In our case, the resonant coherent excitations of the graphene layers allow the enhanced transmission of photons through the central, classically forbidden region for photons, in direct analogy with the metallic case. In the propagating region, the strongly quenched transmission turns into perfect transmission at sharply peaked resonances related to the original Fabry-Pérot resonances, where graphene’s response function is given by the typical Fano lineshape due to the nearly discrete na-

ture of the spectrum in the central slab.

The Letter is organized as follows. We first study the retardation limit and its effect on the GP dispersion for single-layer graphene. Then we consider the retardation regime for double-layer graphene separating different dielectric media where extraordinary transmission takes place. Finally we summarize our results and an appendix details the GPs dispersion relation for the double-layer arrangement in the retardation limit.

Retardation limit. Single-layer graphene. – The standard expression for a 2d plasmon, $\omega_p \propto \sqrt{q}$, assumes instantaneous Coulomb coupling between charges. [20, 21] Therefore, it cannot be correct when the nominal plasmon dispersion meets the light-cone, $\omega_p \lesssim cq$. This is the regime where retardation effects matter and strong light-graphene interaction takes place, as we now show.

Consider a graphene layer sandwiched between two dielectrics with permittivities $\epsilon_{1,2} = \epsilon_{1,2}\epsilon_0$ and $\epsilon_1 > \epsilon_2$. The longitudinal current response to an (in-plane) longitudinal, external vector potential is given by the standard RPA expression

$$\chi_l = \frac{\chi_l^o}{1 - e^2 d_l \chi_l^o}, \quad (1)$$

where $\chi_l = \mathcal{G}_{jj}$ is the retarded Green function for the longitudinal current, χ_l^o its non-interacting (bare) version, and $d_l = \mathcal{G}_{AA}$ that of the (in-plane) longitudinal vector potential (in the absence of graphene). For graphene, we use the well-known results [20, 21, 37] for χ_l^o , whereas for the photon field, one straightforwardly finds [15] $d_l = \frac{q'_1 q'_2 \omega^{-2}}{\epsilon_2 q'_1 + \epsilon_1 q'_2}$, with $q'_i = \sqrt{q^2 - (\omega/c)^2 \epsilon_i}$.

GPs are the poles of Eq. 1, leading to the following (implicit) dispersion relation, including retardation

$$\omega^2 = e^2 \frac{q'_1 q'_2}{\epsilon_2 q'_1 + \epsilon_1 q'_2} \chi_l^o. \quad (2)$$

In the unretarded limit, $c \rightarrow \infty$, this gives the known square-root dispersion. In contrast, the exact solution replaces this behavior with a linear dispersion which merges with the slower medium (1) light-cone below a characteristic crossover frequency, as illustrated in Fig. 1 (left panel), and summarized as follows:

$$\left(\frac{\omega}{\omega_F}\right)^2 = \begin{cases} \left(\frac{4\alpha_g}{\epsilon_1 + \epsilon_2}\right) \left(\frac{q}{k_F}\right), & \omega \gtrsim \omega_c \\ \left(\frac{c_1}{v}\right)^2 \left(\frac{q}{k_F}\right)^2, & \omega \lesssim \omega_c \end{cases}, \quad (3)$$

where ω_F , k_F and v are graphene's Fermi frequency, Fermi momentum and Fermi velocity, $c_1 = c/\sqrt{\epsilon_1}$ is medium 1 (slower) light velocity, and $\alpha_g = \frac{e}{v}\alpha$ represents graphene fine structure constant. The crossover between regimes takes place for frequencies which roughly corresponds to the intersection of the unretarded GP and light-cone dispersions. This scale is given by $\omega_c \sim \alpha\omega_F$ for reasonable dielectric constants. Typical frequencies are $\nu_c \sim 200$ GHz

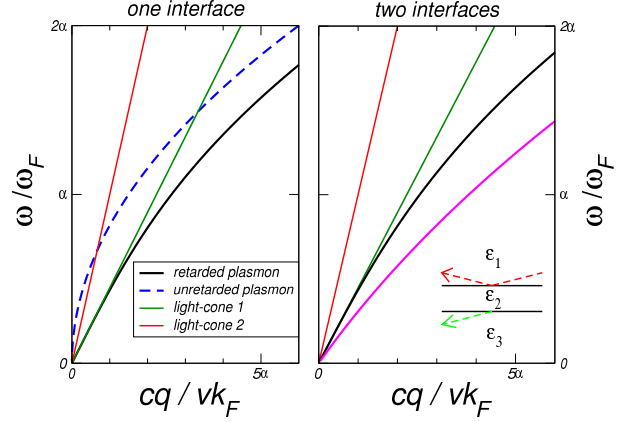


Fig. 1: Left panel: Longitudinal plasmon exact dispersion relation (black continuous line), compared to the instantaneous approximation (blue dashed line) for doped graphene between medium 1 ($\epsilon_1 = 5$) and medium 2 ($\epsilon_2 = 1$), light-cones also shown. Right panel: As in left panel for the double-layer graphene showing the in-phase (upper curve, black) and out-of-phase (lower curve, magenta) plasmons for $\epsilon_3 = \epsilon_1$ and layer separation $\tilde{z} = \tilde{z}_c/2$. Inset: schematic geometry and transmission setup.

for doping level $n \sim 10^{12} \text{ cm}^{-2}$, $\nu_c \sim 600$ GHz for doping level $n \sim 10^{13} \text{ cm}^{-2}$, reaching the technologically important THz regime for $n \sim 10^{14} \text{ cm}^{-2}$.

Therefore, for $\omega \lesssim \omega_c$ retardation always matters. Not surprisingly, this linear regime is also the region of strong graphene-light coupling. This is immediately seen by looking at the reflection and transmission amplitudes for the (in-plane) longitudinal vector potential upon passing from medium i to j , given by

$$r_{ij} = \frac{\epsilon_i q'_j - \epsilon_j q'_i + e^2 q'_i q'_j \chi_l^o \omega^{-2}}{\epsilon_i q'_j + \epsilon_j q'_i - e^2 q'_i q'_j \chi_l^o \omega^{-2}}, \quad (4)$$

$$t_{ij} = 1 + r_{ij}$$

For interband transitions at frequencies above $2\omega_F$, graphene terms in Eq. 4 are minute, leading to the universal 2.3% weak absorption in vacuum, for instance. On the other hand, for frequencies below ω_c , graphene response starts to dominate in Eq. 4 implying strong radiation-graphene coupling. For instance, in the limit $\omega \ll \omega_c$ the reflection amplitude becomes

$$r = -1 + \mathcal{O}\left(\frac{\omega}{\omega_c}\right). \quad (5)$$

$r = -1$ implies perfect reflection or, equivalently, a zero photon field at graphene position as a boundary condition. Therefore, the (small) parameter $\frac{\omega}{\omega_c} \sim \frac{\omega}{\alpha\omega_F}$ of our strong coupling regime also measures the departure from this zero-field boundary condition.

Double-layer graphene. Extraordinary transmission. – We consider two identically doped graphene

sheets, separating three dielectrics with permittivities $\epsilon_{1,2,3}$, see Fig. 1 (right panel), and impose left-right symmetry choosing $\epsilon_2 < \epsilon_1 = \epsilon_3$. Under these conditions, for large enough incident angles the central region does not support propagating modes: light must *tunnel* through this evanescent region. Doped graphene enhanced response in the retardation regime can make this tunneling *perfect*, as we will show.

Reflection and transmission coefficients can be obtained from the corresponding amplitudes, written as

$$\begin{aligned} \tilde{r}_{1,3} &= r_{12} + \frac{t_{12}r_{23}t_{21}e^{-2q'_2z}}{1 - r_{21}r_{23}e^{-2q'_2z}}, \\ \tilde{t}_{1,3} &= \frac{t_{12}t_{23}e^{-q'_2z}}{1 - r_{21}r_{23}e^{-2q'_2z}}, \end{aligned} \quad (6)$$

for light incoming from medium 1 and being transmitted to medium 3 (see Fig. 1 inset), with t_{ij} and r_{ij} taken from Eq. 4.

In order to display the connection between light propagation and graphene behavior, we also calculate the double-layer (longitudinal) current-current response, given by the following matrix generalization of Eq. 1

$$\chi_l = (\mathbf{1} - e^2 \chi_l^o \mathbf{d}_l)^{-1} \chi_l^o, \quad (7)$$

with the 2x2 matrix $\chi_l^o = \text{diag}(\chi_1^o, \chi_2^o)$ representing the non-interacting (longitudinal) response of graphene layers 1 and 2, whereas the photonic matrix $\mathbf{d} = (d_{ij})$ is given by $d_{11} = d_1(1 + \tilde{r}_{1,3}^o)$, $d_{22} = d_3(1 + \tilde{r}_{3,1}^o)$, and $d_{12} = d_1 \tilde{t}_{1,3}^o = d_3 \tilde{t}_{3,1}^o = d_{21}$. Here, $d_1 = \frac{q'_1}{2\epsilon_1\omega^2}$, $d_3 = \frac{q'_3}{2\epsilon_3\omega^2}$, and $\tilde{r}_{i,j}^o$ ($\tilde{t}_{i,j}^o$) correspond to the expressions of Eq. 6 evaluated for the dielectric geometry of Fig. 1, but without graphene layers ($\chi_l^o = 0$ in Eq. 4). For our left-right symmetric arrangement, the in-phase and out-of-phase components of graphene currents, $j_{\pm} = j_1 \pm j_2$, diagonalize χ_l , with corresponding (complex) eigenvalues that we denote by χ_{++} and χ_{--} , respectively.

Genuine (non radiative) GPs correspond to the poles of χ_l in the totally evanescent regime, that is, the region to the right of the slower light-cone in Fig. 1. In the Appendix we show that there always are two GPs, one for each component of the response. The in-phase GP (χ_{++}) merges with the corresponding limiting light-cone, whereas the out-of-phase GP (χ_{--}) either merges with the light-cone or develops its own linear dispersion at slower velocity if the separation between layers is below a critical value $\tilde{z}_c = z_c k_F$, with $\tilde{z}_c = \frac{\epsilon_2}{\epsilon_1 - \epsilon_2} \frac{c}{2v\alpha}$. Both are shown in Fig. 1 (right panel) where we have used $\tilde{z} = \tilde{z}_c/2$, and permittivities $\epsilon_2 = 1$ (vacuum) and $\epsilon_1 = \epsilon_3 = 5$, a representative value for common substrates. For bulk BN, we have, e.g., $\epsilon_{1,3} \sim 5$, whereas $\epsilon_{1,3} \sim 4$ for few layer BN or SiO₂.

Though GPs remain in the evanescent region of both media, the presence of graphene also strongly affects propagating light, leading to resonances with perfect transmission. At first glance, this statement seems incompatible

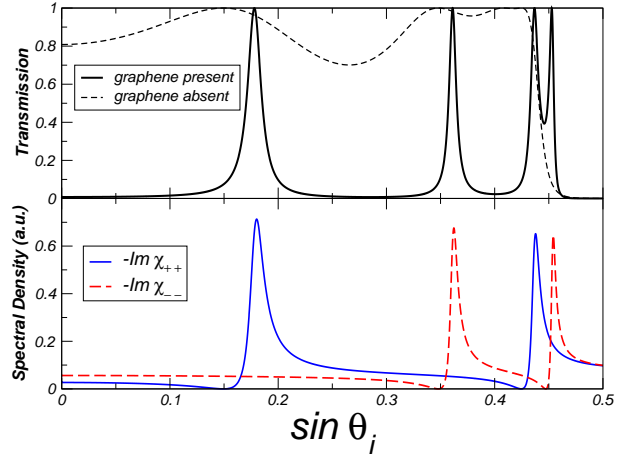


Fig. 2: Top panel: Transmission as a function of incoming angle for frequency $\omega = (\alpha/2)\omega_F$ and double-layer graphene separation $z k_F = 20 c/(v\alpha)$ for permittivities $\epsilon_{1,3} = 5$, $\epsilon_2 = 1$. Dashed (black) line: same as before in the absence of graphene. Bottom panel: Spectral density of the in-phase (solid, blue line) and out-of-phase (dashed, red line) double-layer graphene response.

with the (almost) perfect reflective character of a graphene layer in our strong coupling regime. Yet, the zero field boundary condition also decouples the photon field in the central slab from the propagating modes outside, leading to the standard discrete spectrum for a particle in a box. Now, the small parameter $\frac{\omega}{\omega_c} \sim \frac{\omega}{\alpha\omega_F}$ measuring the departure from perfect reflection is also a measure of the (small) coupling between the discrete modes of the central slab and the propagating modes outside, leading to (radiative) resonances. Drastic changes are expected close to these resonances and, indeed, we will see that the otherwise expected strong reflection turns into perfect transmission.

These resonances are shown in Fig. 2 (top panel), where we present the transmission for layer's separation $z k_F = 20 c/(v\alpha)$ and frequency $\omega = (\alpha/2)\omega_F$. For a doping level of $n \sim 10^{12} \text{cm}^{-2}$, this would imply a frequency $\nu \sim 100 \text{GHz}$, and separation $z \sim 5 \times 10^{-3} \text{m}$. For $n \sim 10^{14} \text{cm}^{-2}$, we have $\nu \sim 1 \text{THz}$, and $z \sim 5 \times 10^{-4} \text{m}$. Although the existence of perfect transmission at Fabry-Pérot-like resonances is generic for this geometry even without graphene (see dotted line in top panel of Fig.2), these resonances are sharply modified by its presence. The otherwise strongly reflective graphene confines the transmission to narrow resonances close to the region where the almost discrete central slab modes are excited. The narrow width of these resonances is a measure of the long lifetime of the central photonic modes, weakly decaying into the radiative modes outside. A direct evidence of the role of these (almost) discrete spectrum is provided by the spectral densities of the in-phase (χ_{++}) and out-of-phase (χ_{--}) graphene response, also shown in Fig. 2 (bottom panel). Up to an overall scale, these spectral densities co-

incide with the spectral densities of the photonic field and, therefore, the sharp resonances in graphene match the expected sharp spectral densities of weakly decaying, almost discrete photonic modes. Notice the one-to-one correspondence between response and transmission peaks, emphasizing the role of these modes in overturning the otherwise generic strong reflection of graphene in the strong coupling limit.

The spectral functions of the bottom panel of Fig. 2 exhibit a marked asymmetric Fano-like profile, vanishing precisely where grapheneless transmission is one. This Fano-like profile can be expected, given the key role played by the almost discrete modes of the central slab. It can be quantitatively explained noticing that

$$\chi_{\pm\pm} \sim \frac{1}{1 - e^2 \chi_l^o(d_{11} \pm d_{12})}, \quad (8)$$

but the photon propagator in the absence of graphene vanishes at the corresponding grapheneless resonances as

$$d_{11} \pm d_{12} \sim a(\delta s) + ib(\delta s)^2, \quad (9)$$

where a and b are real constants, and δs is the departure of $\sin(\theta_i)$ from the value corresponding to the discrete modes upon strictly enforcing zero-field boundary conditions, given by $\exp(-2q'_2 z) = 1$. Notice that this zero-field boundary condition for discrete modes in the presence of graphene coincides with the perfect transmission condition in the absence of graphene, explaining the vicinity of both points. The small shift of the actual solution being the consequence of the small leaking of discrete modes into the outside continuum. This leaking also accounts for the small width of the resonance, and leads to a characteristic resonance asymmetry, given by $-\text{Im}\chi_{\pm\pm} \sim \frac{(\delta s)^2}{(\delta s - s_*)^2 + l^2(\delta s)^4}$, where $s_* \sim \frac{\omega/\omega_F}{\alpha l}$ is the resonance shift from the nominal discrete modes graphene, playing the role of small parameter in the strong coupling regime, and l being (up to a factor of order one) the central slab width in units of the minimum required for the emergence of the first nominal discrete mode. This expression can be approximately recast in the more common Fano lineshape [38],

$$-\text{Im}\chi_{\pm\pm} \sim \frac{(Q\gamma/2 + \delta s')^2}{(\delta s')^2 + (\gamma/2)^2}, \quad (10)$$

with the identifications $\delta s' = \delta s - s_*$, the width $\gamma \sim ls_*^2$, and the Fano asymmetry parameter $Q = \frac{2s_*}{\gamma}$ with value $Q \sim 2 - 3$, for fig. 2 (bottom panel).

Interestingly, the rightmost resonance in Fig. 2 occurs for $\sin\theta_i > 1/\sqrt{5} \sim 0.447$, that is, in the evanescent regime for medium 2. In fact, we can tune the arrangement to make this last resonance the only one present. This is shown in Fig. 3, where we present the transmission calculated with the same frequency as before $\omega = (\alpha/2)\omega_F$, but for three shorter separations given by $z_1 k_F = 2c/(v\alpha)$, $z_2 = z_1/5$, and $z_3 = z_1/10$

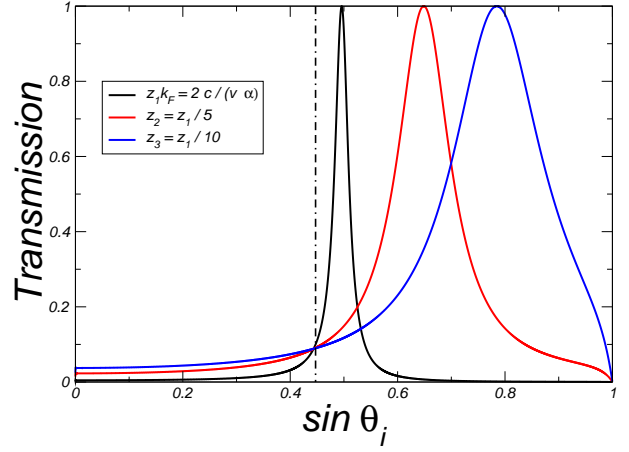


Fig. 3: Transmission as a function of incoming angle for frequency $\omega = (\alpha/2)\omega_F$, permittivities $\epsilon_{1,3} = 5$, $\epsilon_2 = 1$, and double-layer graphene separations: $z_1 k_F = 2c/(v\alpha)$ (black), $z_2 = z_1/5$ (red), and $z_3 = z_1/10$ (blue). The vertical dashed line marks the onset of the evanescent regime in the central slab.

($\nu \sim 100$ GHz and $z_1 \sim 5 \times 10^{-4}$ m for $n \sim 10^{12}$ cm $^{-2}$). One can observe a perfect transmission peak within the classically forbidden region for photons. This resonance is rather sharp close to the propagating boundary, moving deeper into the evanescent region and broadening with decreasing double-layer separation. Notice that, for the cases shown in Fig. 3, the transparency window is virtually confined to the evanescent regime. Although a finite photon tunneling always exists, the fact that the transmission becomes perfect in the evanescent region [39] is entirely due to the presence of doped graphene sheets, and is associated with a resonance in their out-of-phase response (see bottom panel of Fig. 2). This perfect transmission peak within the evanescent region extends all the way down to zero frequency, as shown in the top left panel of Fig. 4. For higher frequencies, this resonance approaches the upper light-cone and merges with the lowest propagating Fabry-Pérot like resonance, as seen in the bottom left panel of Fig. 4.

Our aim so far has been to expose the strong light-graphene coupling of the retardation regime in a simple manner. Therefore, we have ignored absorption. Graphene losses will degrade the perfect nature of transmission, making the possible observation of coherent effects more likely in reflection rather than transmission. Although we are not aware of any intrinsic limitation in the minimization of losses attainable in doped graphene, the low frequencies of the strong-coupling regime might pose a severe handicap. Nevertheless, absorption opens new possibilities: the sharp response of graphene in the absence of absorption suggests a correspondingly enhanced absorption when losses are allowed. This is the case as the upper right panel of Fig. 4 shows, where the ab-

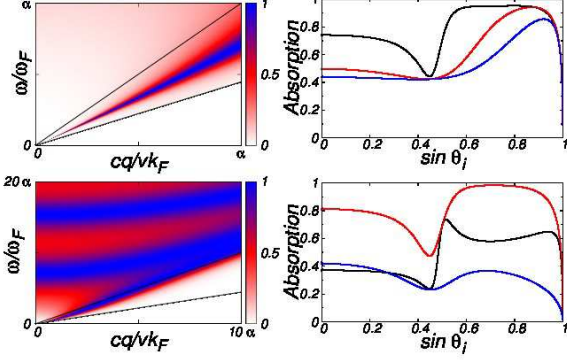


Fig. 4: Top left panel: Transmission in the ω - q plane showing the perfect resonance within the evanescent region for double-layer separation corresponding to $z_2 k_F = 2c/(5v\alpha)$. Bottom left panel: As in top left panel for an extended region of the ω - q plane to include additional Fabry-Pérot-like resonances. Top right panel: Absorption when graphene losses are included with $\omega\tau = 0.65$ for the same double-layer separations (and colors) as in Fig. 3. Bottom right panel: Absorption for fixed double-layer separation $z_1 k_F = 2c/(v\alpha)$ and graphene losses $\omega\tau = 2$ (black), $\omega\tau = 0.5$ (red), and $\omega\tau = 0.05$ (blue).

sorption for a lifetime $\tau \sim 10^{-12}s$, present in suspended graphene and corresponding to $\omega\tau = 0.65$, is plotted for the same double-layer separations of Fig. 3. Indeed, one observes an overall high absorption, reaching values above 90% precisely in the evanescent region. From this perspective, our arrangement is closely connected to that of Ref. [40], providing a complementary and potentially simpler alternative to absorption enhancement based on periodic patterning [29–31]. It is similar, though, to the previously suggested enhanced absorption of graphene placed in a (double) Fabry-Pérot cavity. [41, 42]

In the bottom right panel of Fig. 4, the absorption for different intrinsic damping rates corresponding to $\omega\tau = 2, 0.5, 0.05$ is shown where the last value would assume a phenomenological relaxation rate γ of the polarization with $\hbar\gamma \sim 10\text{meV}$, present in graphene on a SiO_2 -substrate. Notice that the double-layer absorption can display a non-monotonous behavior with the intrinsic single-layer graphene losses, providing a richer degree of control.

Summary. – We have studied the retardation regime of doped graphene plasmons, given by $(\omega/\omega_F) \lesssim \alpha$. Apart from modifying the unretarded GP dispersion behavior from \sqrt{q} to q , such a limit marks the onset of strong radiation-graphene coupling and we have exhibited such enhancement in the simplest double-layer arrangement. i) We first observed that the transmission is strongly quenched except at sharply peaked resonances, consistent with the nearly discrete spectrum of the strongly confined field in the central slab brought about by graphene, whose

response function is given by the typical Fano lineshape. ii) We also discussed that the transmission, perfect if losses are ignored, can be confined to the classically forbidden region for photons between graphene layers, providing a direct analog of the extraordinary transmission through perforated metals in a conceptually simpler setup. iii) Finally, we showed that enhanced transmission becomes increased absorption when losses are allowed, displaying non-monotonous behavior. Graphene’s doping tunability in this or similar setups should thus open up new ways to efficiently control the flow and/or absorption of radiation.

This work has been supported by FCT via grant PTDC/FIS/101434/2008 and by MICINN via grant FIS2010-21883-C02-02.

Appendix. – We outline here the calculation of double-layer GPs in the retarded regime. We take $\epsilon_3 = \epsilon_1 > \epsilon_2$. Therefore, genuine GPs are the response poles located to the right of the slower (outer media) light-cone. These are given by the solutions of

$$1 \mp r_{21} e^{-q'_2 z} = 0, \quad (11)$$

corresponding to the in-phase (χ_{++}) and out-of-phase (χ_{--}) response components, respectively. Taking r_{21} from Eq. 4 deep into the retarded regime, one finds the in-phase GP as

$$\epsilon_1 \tilde{\omega}_+^2 \rightarrow 4\pi\alpha_g \tilde{\chi}^o \tilde{q}'_1, \quad (12)$$

where we have used dimensionless magnitudes: $\tilde{\omega} = \omega/\omega_F$, $\alpha_g = \tilde{c}\alpha$, $\tilde{c} = c/v$, $\tilde{c}_i^2 = \tilde{c}^2/\epsilon_i$, $\tilde{q} = q/k_F$, $\tilde{q}'_i = \sqrt{\tilde{q}^2 - \tilde{\omega}^2/\tilde{c}_i^2}$, with single-layer graphene response, $\tilde{\chi}^o = \pi^{-1}$, taken in the local approximation, excellent for the retarded regime. In this limit, $\tilde{\omega}_+$ coincides with the GP pole of an isolated graphene layer in the boundary between two (semi-infinite) media 1 and 2. Therefore, one easily sees that it merges asymptotically with the outer media light-cone, as in Eq. 3:

$$\tilde{\omega}_+ = \tilde{c}_1 \tilde{q} + \mathcal{O}(\tilde{q}^3). \quad (13)$$

Analyzing the *plus* Eq. 11 for the out-of-phase GP, a critical layer separation emerges, z_c , given by

$$z_c k_F = \tilde{z}_c = \frac{\epsilon_2}{2(\epsilon_1 - \epsilon_2)} \frac{\tilde{c}}{\alpha}, \quad (14)$$

that separates the following two regimes

$$\tilde{\omega}_- = \begin{cases} \tilde{c}_1 \tilde{q} + \mathcal{O}(\tilde{q}^3), & \tilde{z} > \tilde{z}_c \\ \tilde{v}_- \tilde{q} + \mathcal{O}(\tilde{q}^3), & \tilde{z} < \tilde{z}_c \end{cases}, \quad (15)$$

where

$$\tilde{v}_-^2 = \frac{\tilde{c}_1^2}{1 + (1 - \frac{\epsilon_2}{\epsilon_1})(\frac{\tilde{z}_c}{\tilde{z}} - 1)}. \quad (16)$$

We conclude that the out-of-phase GP develops a linear dispersion relation that either merges with the outer media light-cone (and, therefore, with $\tilde{\omega}_+$ from below) for $\tilde{z} > \tilde{z}_c$, or shows a lower velocity $\tilde{v}_- < \tilde{c}_1$ for $\tilde{z} < \tilde{z}_c$, as stated in the paper.

REFERENCES

- [1] GEIM A. K., *Science*, **324** (2009) 1530.
- [2] NAIR R. R., BLAKE P., GRIGORENKO A. N., NOVOSELOV K. S., BOOTH T. J., STAUBER T., PERES N. M. R. and GEIM A. K., *Science*, **320** (2008) 1308.
- [3] MAK K. F., SFEIR M. Y., WU Y., LUI C. H., MISEWICH J. A. and HEINZ T. F., *Phys. Rev. Lett.*, **101** (2008) 196405.
- [4] BAE S. *et al.*, *Nature Nanotechnology*, **5** (2010) 574.
- [5] BONACCORSO F., SUN Z., HASAN T. and FERRARI A. C., *Nat. Photonics*, **4** (2010) 611.
- [6] MUELLER T., XIA F. and AVOURIS P., *Nature Photonics*, **4** (2010) 297.
- [7] LIU M. *et al.*, *Nature*, **474** (2011) 64.
- [8] SUN Z. *et al.*, *ACS Nano*, **4** (2010) 803.
- [9] TREOSSI E., MELUCCI M., LISCIO A., GAZZANO M., SAMORI P. and PALERMO V., *J. Am. Chem. Soc.*, **131** (2009) 15576.
- [10] KIM J., COTE L. J., KIM F. and HUANG J., *J. Am. Chem. Soc.*, **132** (2010) 260.
- [11] CHEN Z., BERCIAUD S., NUCKOLLS C., HEINZ T. F. and BRUS L. E., *ACS Nano*, **4** (2010) 2964.
- [12] LOH K. P., BAO Q., EDA G. and CHHOWALLA M., *Nat. Chem.*, **2** (2010) 1015.
- [13] SWATHI R. S. and SEBASTIAN K. L., *J. Chem. Phys.*, **130** (2009) 086101.
- [14] VELIZHANIN K. A. and EFIMOV A., *Phys. Rev. B*, **84** (2011) 085401.
- [15] GÓMEZ-SANTOS G. and STAUBER T., *Phys. Rev. B*, **84** (2011) 165438.
- [16] JABLAN M., BULJAN H. and SOLJAČIĆ M., *Phys. Rev. B*, **80** (2009) 245435.
- [17] VAKIL A. and ENGHETA N., *Science*, **332** (2011) 1291.
- [18] KOPPENS F. H. L., CHANG D. E. and GARCÍA DE ABAJO F. J., *Nano Lett.*, **11** (2011) 3370.
- [19] NIKITIN A. Y., GUINEA F., GARCÍA-VIDAL F. J. and MARTÍN-MORENO L., *Phys. Rev. B*, **84** (2011) 161407(R).
- [20] WUNSCH B., STAUBER T., SOLS F. and GUINEA F., *New J. Phys.*, **8** (2006) 318.
- [21] HWANG E. H. and SARMA S. D., *Phys. Rev. B*, **75** (2007) 205418.
- [22] BARLAS Y., PEREG-BARNEA T., POLINI M., ASGARI R. and MACDONALD A. H., *Phys. Rev. Lett.*, **98** (2007) 236601.
- [23] LIU Y., WILLIS R. F., EMTSEV K. V. and SEYLLER T., *Phys. Rev. B*, **78** (2008) 201403.
- [24] TEGENKAMP C., PFNÜR H., LANGER T., BARINGHAUS J. and SCHUMACHER H. W., *J. Phys. Condens. Matter*, **23** (2011) 012001.
- [25] FEI Z. *et al.*, *Nano Lett.*, **1** (2011) 470.
- [26] CHEN J., BADIOLI M., ALONSO-GONZÁLEZ P., THONGRATTANASIRI S., HUTH F., OSMOND J., SPASENOVIC M., CENTENO A., PESQUERA A., GODIGNON P., ZURUTUZA A., CAMARA N., GARCIA DE ABAJO J., HILLENBRAND R. and KOPPENS F., *Nature*, **487** (2012) 77.
- [27] FEI Z., RODIN A. S., ANDREEV G. O., BAO W., MCLEOD A. S., WAGNER M., ZHANG L. M., ZHAO Z., DOMINGUEZ G., THIEMENS M., FOGLER M. M., CASTRO-NETO A. H., LAU C. N., KEILMANN F. and BASOV D. N., *Nature*, **487** (2012) 82.
- [28] CHRISTENSEN J., MANJAVACAS A., THONGRATTANASIRI S., KOPPENS F. H. L. and GARCÍA DE ABAJO F. J., *ACS Nano*, **6** (2012) 431.
- [29] JU L., GENG B., HORNG J., GIRIT C., MARTIN M., HAO Z., BECHTEL H. A., LIANG X., ZETTL A., SHEN Y. R. and WANG F., *Nat. Nanotechnol.*, **6** (2011) 630.
- [30] ECHTERMEYER T., BRITNELL L., JASNOS P., LOMBARDO A., GORBACHEV R., GRIGORENKO A., GEIM A., FERRARI A. and NOVOSELOV K., *Nat. Comm.*, **2** (2011) 458.
- [31] THONGRATTANASIRI S., KOPPENS F. H. L. and GARCÍA DE ABAJO F. J., *Phys. Rev. Lett.*, **108** (2012) 047401.
- [32] HWANG E. H. and SARMA S. D., *Phys. Rev. B*, **80** (2009) 205405.
- [33] STAUBER T. and GÓMEZ-SANTOS G., *Phys. Rev. B*, **85** (2012) 075410.
- [34] EBBESEN T. W., LEZEC H. J., GHAEMI H. F., THIO T. and WOLFF P. A., *Nature*, **391** (1998) 667.
- [35] MARTÍN-MORENO L., GARCÍA-VIDAL F. J., LEZEC H. J., PELLERIN K. M., THIO T., PENDRY J. B. and EBBESEN T. W., *Phys. Rev. Lett.*, **86** (2001) 1114.
- [36] GARCIA-VIDAL F. J., MARTIN-MORENO L., EBBESEN T. W. and KUIPERS L., *Rev. Mod. Phys.*, **82** (2010) 729.
- [37] STAUBER T. and GÓMEZ-SANTOS G., *Phys. Rev. B*, **82** (2010) 155412.
- [38] FANO U., *Phys. Rev.*, **124** (1961) 1866.
- [39] GARCÍA DE ABAJO F. J., GÓMEZ-SANTOS G., BLANCO L. A., BORISOV A. G. and SHABANOV S. V., *Phys. Rev. Lett.*, **95** (2005) 067403.
- [40] BLUDOV Y. V., VASILEVSKIY M. I. and PERES N. M. R., *Europhys. Lett.*, **92** (2010) 68001.
- [41] FURCHI M., URICH A., POSPISCHIL P., LILLEY G., UNTERRAINER K., DETZ H., KLANG P., ANDREWS A. M., SCHRENK W., STRASSER G. and MÜLLER T., *Nano Lett.*, **12** (2012) 2773.
- [42] FERREIRA A., PERES N. M. R., RIBEIRO R. M. and STAUBER T., *Phys. Rev. B*, **85** (2012) 115438.